Inorganic Chemistry

Article

pubs.acs.org/IC

Good Thermoelectric Performance in Strongly Correlated System $SnCCo_3$ with Antiperovskite Structure

Shuai Lin,[†] Peng Tong,*[,†] Bosen Wang,[†] Jianchao Lin,[†] Yanan Huang,[†] and Yuping Sun*[,†,‡,§]

[†]Key Laboratory of Materials Physics, Institute of Solid State Physics and [‡]High Magnetic Field Laboratory, Chinese Academy of Sciences, Hefei 230031, People's Republic of China

[§]University of Science and Technology of China, Hefei 230026, People's Republic of China

ABSTRACT: We report the magnetic, electrical, and thermoelectric properties of $SnCCo_3$, where good thermoelectric performance [figure of merit $ZT \sim 0.035(2)$, 258 K] and strong electron correlation (Kadowaki–Woods ratio $R_{KW} \sim 4a_0$) are observed. The thermoelectric properties of $ACCo_3$ (A = Al, Ga, Ge) and $SnCM_3$ (M = Mn, Fe) were also investigated for comparison. As a result, the ZT value of $SnCCo_3$ is the largest among all of those samples, which is mainly attributed to the large Seebeck coefficient caused by the strong electron correlation and low carrier density. Moreover, the ZT value can be effectively enhanced by proper chemical doping in $SnCCo_3$.

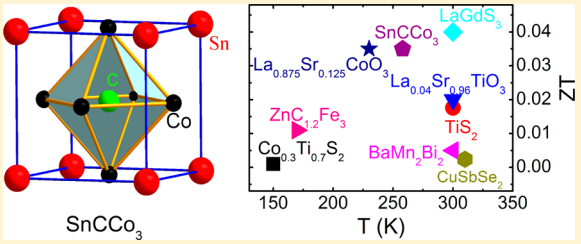

1. INTRODUCTION

Thermoelectric (TE) materials with high figure of merit ($ZT = \alpha^2 T/\rho\kappa$, where α is the Seebeck coefficient, ρ is the electrical resistivity, and κ is the thermal conductivity) have been attracting significant attention because of potential applications in heat-electricity conversion at high temperatures and TE cooling below or around room temperature.[1] For most of the TE materials with high ZT such as Si–Ge, Pt(Fe)Sb_2, $Hg_{1-x}Cd_xTe$, $AgSbTe_2$, PbTe(Se), $Na_xCo_2O_4$, and $CoSb_3$,[2] the optimum operating temperatures are above 400 K, where the TE materials are used for heat-electricity conversion via the Seebeck effect.[1,3] On the other hand, below or around room temperature, a good TE property is very important for TE cooling using the Peltier effect. A high ZT value usually requires a high Seebeck coefficient, which can be found in a strong correlation system such as $FeSb_2$ (10000 μV/K, 50 K), $CeAl_3$ (42 μV/K, 50 K), and $CePb_3$ (40 μV/K, 20 K).[3,4] This raises considerable interest in exploring the synthesis of strongly correlated electron materials.

Since the first antiperovskite superconductor $MgCNi_3$ was reported in 2001,[5] the antiperovskite structural compounds AXM_3 (A = Ga, Al, Sn, Zn, Cu, In, Ge, etc.; X = C, N; M = Mn, Fe, Ni, etc.) have been studied extensively in the past decade and plenty of interesting physical properties and potential functionalities such as magnetic frustration,[6] giant magnetoresistance,[7−9] magnetocaloric effect,[10,11] negative thermal expansion,[12−14] and nearly zero temperature coefficient of resistivity have been found.[15−17] However, there are relatively fewer reports of the TE properties in the antiperovskite system. Besides, recent investigations of AXM_3 mainly focused on the Mn-, Fe-, and Ni-based antiperovskite compounds.[5−17] Up to now, there is still no detailed research on Co-based antiperovskite compounds ($AXCo_3$) except for the $AlCCo_3$ system.[18−20] Recently, the Seebeck coefficient of $AlCCo_{3-x}M_x$ (M = Fe, Ni) has been systematically studied, and the maximum Seebeck coefficients of 32.6 and 26.9 μV/K were observed around 873 K for $AlCCo_{3-x}Fe_x$ and $AlCCo_{3-x}Ni_x$, respectively.[20] The above results indicate that a large TE effect may occur in other Co-based antiperovskite compounds and could be tuned by chemical doping. Therefore, it is of interest and importance to investigate the TE properties of Co-based antiperovskite compounds $AXCo_3$ and doped samples.

Here, we systematically study the TE properties of Co-based antiperovskite carbides $ACCo_3$ (A = Al, Ga, Ge, Sn) and isostructural antiperovskite carbides $SnCM_3$ (M = Mn, Fe). As a consequence, a good TE performance [$ZT = 0.035(2)$, 258 K] accompanied with strong electron correlation is obtained in $SnCCo_3$. This strong electron correlation is closely related to the large Seebeck coefficient and even to the large ZT value of $SnCCo_3$. In addition, we also observe that chemical doping is an effective way to tune the ZT value in the $SnCCo_3$ system.

2. EXPERIMENTAL DETAILS

Polycrystalline samples of $SnCM_3$ (M = Mn, Fe, Co), $ACCo_3$ (A = Al, Ga, Ge, Sn), and $Sn_{1-x}Co_xCCo_3$ and $Sn_{1-x}Sb_xCCo_3$ (x = 0, 0.05, and 0.1) were prepared by a direct solid-state reaction.[10,17] Powders of the corresponding element were mixed in the desired proportions, pressed into pellets (at a pressure of 25 MPa), sealed in evacuated quartz tubes ($\sim 10^{-3}$ Pa), and then annealed at 1023–1073 K for about 5–7 days. After quenching the tubes to room temperature, the products were pulverized, mixed, pressed into pellets, and annealed again at 1073–1173 K for more than 7 days in order to obtain the homogeneous samples. Powder X-ray diffraction (XRD) was performed using a Philips X'pert PRO X-ray diffractometer with Cu Kα radiation (λ = 0.15406 nm) at room temperature. Magnetic measurements were performed on a Quantum Design superconducting quantum interference device magnetometer (SQUID-5T). The electrical/

Received: January 6, 2014
Published: March 25, 2014

   dx.doi.org/10.1021/ic500026t | Inorg. Chem. 2014, 53, 3709–3715

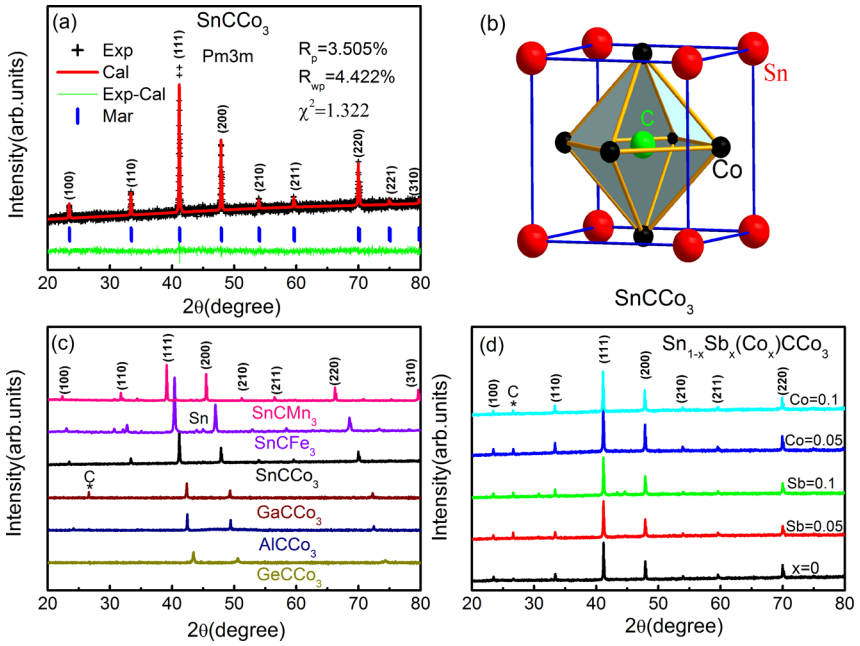

Figure 1. (a) Rietveld refined powder XRD patterns for $SnCCo_3$. The vertical marks indicate the positions of the Bragg peaks, and the solid line at the bottom corresponds to the difference between the experimental and calculated intensities. (b) Crystal structure of $SnCCo_3$. (c) Room-temperature powder XRD for $SnCM_3$ (M = Mn, Fe, Co) and $ACCo_3$ (A = Sn, Ga, Al, Ge). (d) Room-temperature powder XRD for $Sn_{1-x}Co_x(Sb_x)CCo_3$.

thermal transport and specific heat properties were measured on a Quantum Design physical property measurement system (PPMS-9T). The Seebeck coefficient and thermal conductivity were measured using the PPMS configured with the thermal transport option. This measurement was made by attaching four leads to the sample with conducting silver epoxy.

3. RESULTS AND DISCUSSION

Figure 1a shows the Rietveld refinement of the room-temperature powder XRD pattern for $SnCCo_3$, and all of the diffraction peaks could be indexed to the cubic antiperovskite structure (space group: *Pm*3*m*), indicating that our sample $SnCCo_3$ is single phase. Figure 1b displays the sketch map of the crystal structure of $SnCCo_3$. The refined lattice parameter (a) obtained by using a Rietveld refinement technique is 0.38047(3) nm, which is larger than that of the previously reported $SnC_{1-\delta}Co_3$ (~0.378 nm).[21] Parts c and d of Figure 1 reveal the room-temperature XRD patterns for ACM_3 (A = Al, Ga, Ge, Sn; M = Mn, Fe, Co), $Sn_{1-x}Co_xCCo_3$, and $Sn_{1-x}Sb_xCCo_3$ (x = 0, 0.05, and 0.1), respectively. Obviously, all of the samples are single phase with a cubic antiperovskite structure except for a little graphite for $GaCCo_3$ and doped samples and a tiny amount of Sn for $SnCFe_3$.

Figure 2a presents the temperature-dependent magnetization $M(T)$ and inverse susceptibility $\chi^{-1}(T)$ curves of $SnCCo_3$ at a magnetic field of 100 Oe under both zero-field-cooled (ZFC) and field-cooled (FC) processes between 5 and 380 K. As shown in Figure 2a, there exists a sharp decrease of the magnetization in the temperature range of 5−15 K, meaning the occurrence of a magnetic transition. The inset of Figure 2a shows the isothermal magnetization curve $M(H)$ at 5 K, from which we can find that the ground state of $SnCCo_3$ is ferrimagnetic (FIM). That is to say, the magnetic transition in the $M(T)$ curve is a FIM−paramagnetic phase transition. Above 15 K, the $\chi^{-1}(T)$ curve is linear, which can be well fitted by the Curie−Weiss law:

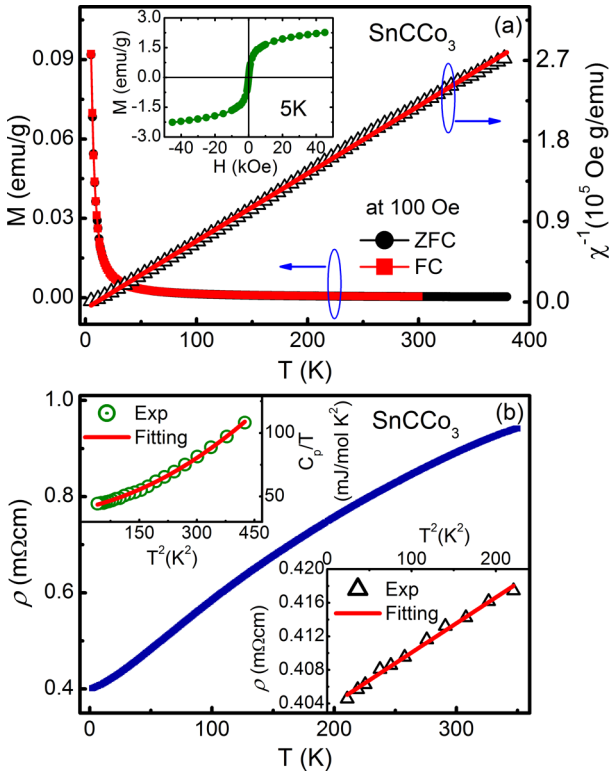

Figure 2. (a) Temperature-dependent magnetization $M(T)$ and inverse susceptibility $\chi^{-1}(T)$ curves at 100 Oe under ZFC/FC processes for $SnCCo_3$. The inset displays the $M(H)$ curve at 5 K. (b) Temperature-dependent resistivity $\rho(T)$ (2−350 K) for $SnCCo_3$. Left inset: Plot of $C_p(T)/T$ versus T^2 below 20 K. The solid line represents the fitting results according to eq 2. Right inset: lower-T $\rho(T)$ data plotted as $\rho(T)$ versus T^2. The solid line is a linear fitting result.

dx.doi.org/10.1021/ic500026t | Inorg. Chem. 2014, 53, 3709−3715

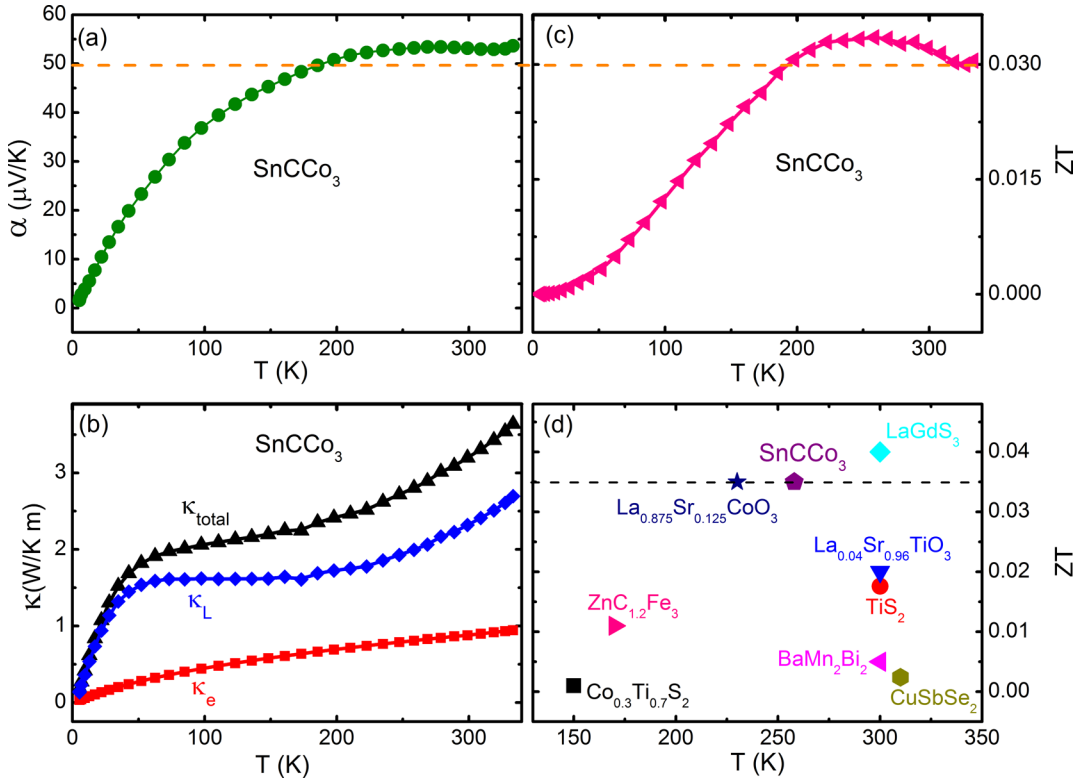

Figure 3. (a) Temperature-dependent Seebeck coefficient $\alpha(T)$ between 5 and 330 K. (b) Temperature dependence of the thermal conductivity $k(T)$, electronic thermal conductivity κ_e, and lattice thermal conductivity κ_L for $SnCCo_3$ in a temperature range of 5−330 K. (c) Dimensionless figure of merit ($ZT = \alpha^2T/\rho k$) plotted as a function of the temperature (5−330 K). (d) Comparison of ZT of $SnCCo_3$ with those of other typical nearly room-temperature TE materials. The dashed line is a guide to the eye.

$$\chi(T)^{-1} = \frac{T - \theta}{C} \quad (1)$$

where C is the Curie constant and θ stands for the Weiss temperature. Correspondingly, we get the values of the parameters as follows: C = 0.405(3) emu·K/mol and θ = 9.74(2) K. The effective magnetic moment per Co atom, μ_{eff}, is estimated as 1.04(3) μ_B from the relationship $\mu_{eff} = 2.83(C/\eta)^{0.5}\mu_B$ (where C is the Curie constant and η is the number of magnetic atoms in a unit cell and is equal to 3 in the present case).[22] This value [μ_{eff} = 1.04(3) μ_B] is less than the local magnetic moment of Co^{2+} (high spin ∼3.87 μ_B) or (low spin ∼1.73 μ_B), meaning that the 3d electrons of Co in $SnCCo_3$ are partly itinerant. Figure 2b shows the temperature dependence of resistivity $\rho(T)$ for $SnCCo_3$ at zero magnetic field between 2 and 350 K. Apparently, the magnitude of $\rho(T)$ increases basically with increasing temperature, indicating a good metallic behavior. As displayed in the right inset of Figure 2b, the low-T resistivity is well fitted by the formula $\rho = \rho_0 + AT^2$ (ρ_0 and A represent the residual resistivity and T^2-term coefficient of the resistivity, respectively) up to 15 K, suggesting a Fermi liquid behavior at low temperatures for $SnCCo_3$. Correspondingly, the fitting values of parameters ρ_0 = 0.4034(2) mΩ·cm and A = 6.576(5) × 10^{-5} mΩ·cm/K^2 are obtained. The left inset of Figure 2b reveals the low-temperature (below 20 K) specific heat $C_P(T)$ of $SnCCo_3$ plotted as $C_P(T)/T$ versus T^2, which can be well expressed by using the following equation:[22]

$$C_P(T)/T = \gamma + \beta T^2 + \delta T^4 \quad (2)$$

where γ (Sommerfeld constant) is the electronic contribution, βT^2 is the phonon contribution, and δT^4 reflects the deviation term. As a result, the fitted values of parameters γ, β, and δ are 40.51(2) mJ/mol·K^2, 0.0663(2) mJ/mol·K^4, and 2.23(3) × 10^{-4} mJ/mol·K^6, respectively. Accordingly, the Debye temperature $\Theta_D = [(n \times 1.94 \times 10^6)/\beta]^{1/3}$ = 527.7(3) K (where n is the number of atoms in a unit cell, and here it is 5) is derived from the value of parameter β for $SnCCo_3$.[22] Generally, the value of the Kadowaki−Woods ratio (R_{KW}), defined as $R_{KW} = A/\gamma^2$ (where A is the T^2-term coefficient of resistivity and γ stands for the Sommerfeld constant of specific heat), is the well-known measure of the electron correlation strength.[22,23] As discussed above for $SnCCo_3$, the values of parameters A and γ are 0.06576(5) μΩ·cm/K^2 and 40.51(2) mJ/mol·K^2, respectively. The calculated R_{KW} of $SnCCo_3$ is 4.01(2) × 10^{-5} μΩ·cm/(mJ/mol·K)^2, which is larger than the universal value of a_0 = 1.0 × 10^{-5}μΩ·cm/(mJ/mol·K)^2 for a strong electron correlation system,[22,23] indicating that $SnCCo_3$ is a strongly correlated system. For comparison, R_{KW} of $SnCCo_3$ (∼4a_0) is larger than those of isostructural $GaCNi_3$ (∼0.72a_0) and $ZnCFe_3$ (∼0.64a_0).[10,22]

Figure 3a displays the temperature-dependent Seebeck coefficient $\alpha(T)$ from 5 to 330 K. Usually, in the single-band model, the sign of $\alpha(T)$ could reflect the types of carriers.[24] Here, in the whole measured temperature range (5−330 K), a positive value of $\alpha(T)$ indicates that the hole-type carriers are dominant in $SnCCo_3$. The magnitude of $\alpha(T)$ increases with increasing temperature first and then decreases gradually after a broad peak of 53 μV/K is reached around 278 K. To the best of our knowledge, this Seebeck coefficient is the largest among antiperovskite compounds.[10,20,22,25] Besides, the Seebeck coefficient of $SnCCo_3$ (≥50 μV/K, 200−330 K) is also larger than those of metal TE materials such as Kondo alloys AuCo

dx.doi.org/10.1021/ic500026t | Inorg. Chem. 2014, 53, 3709−3715

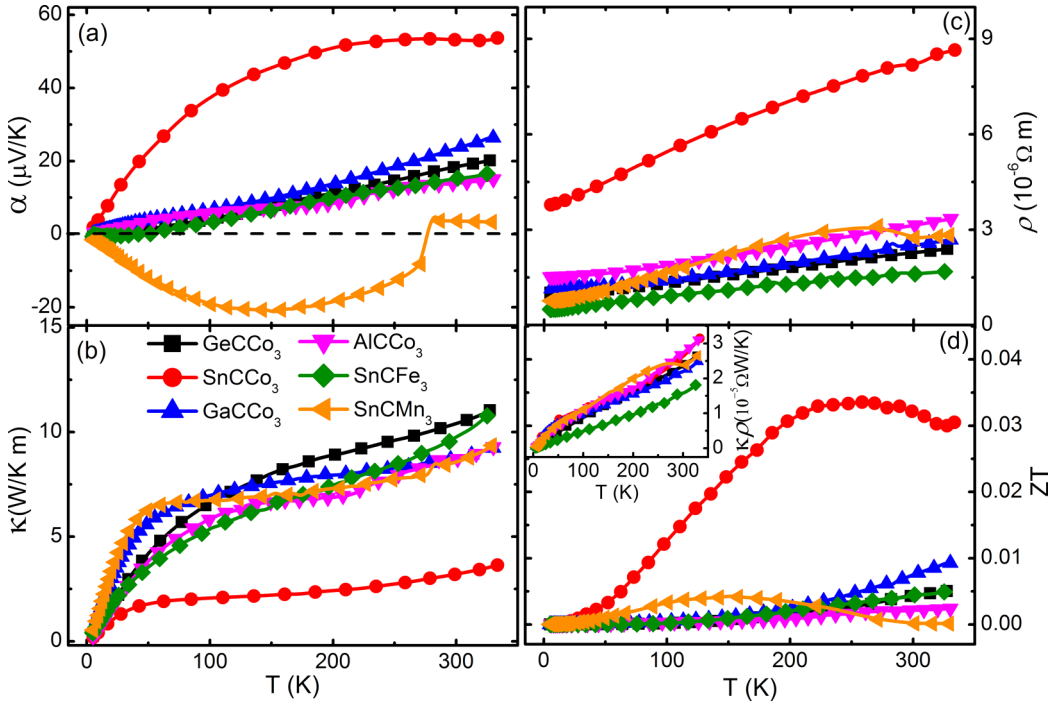

Figure 4. Temperature-dependent $\alpha(T)$, $k(T)$, $\rho(T)$, and ZT(T) curves for $SnCM_3$ (M = Mn, Fe, Co) and $ACCo_3$ (A = Sn, Ga, Al, Ge), respectively: (a) $\alpha(T)$; (b) $k(T)$; (c) $\rho(T)$; (d) ZT(T). The inset shows $k\rho(T)$.

(−42 μV/K, 300 K) and CuFe (−15 μV/K, 20 K) and heavy Fermi metals $CeCu_2Si_2$ (34 μV/K, 200 K), $CeAl_3$ (42 μV/K, 50 K), $CePb_3$ (40 μV/K, 20 K), and $YbInCu_4$ (−30 μV/K, 50 K).[3] In a word, the Seebeck coefficient of $SnCCo_3$ is considerably large in metal TE materials.[3] Figure 3b shows the temperature-dependent thermal conductivity $\kappa(T)$ for $SnCCo_3$ between 5 and 330 K. A broaden peak can be seen around 50 K for $SnCCo_3$, which is similar to those of other antiperovskite compounds.[10,25] In general, the total thermal conductivity can be expressed as a sum of the lattice (κ_L) and electronic (κ_e) terms, i.e., $\kappa(T) = \kappa_L(T) + \kappa_e(T)$. The electronic thermal conductivity κ_e can be estimated based by the Wiedemann−Franz (WF) law [$\kappa_e\rho/T = L_0$, where $L_0 = 2.45 \times 10^{-8}$ W·Ω·K^{-2} is the Lorentz number] and the value of κ_L is obtained in terms of $\kappa(T) - \kappa_e(T)$. For $SnCCo_3$, the values of κ_L and κ_e are separated, and the value of κ_L is larger than that of κ_e in the whole temperature range. Therefore, the peak of $\kappa(T)$ around 50 K is suggested to mainly result from the contribution of $\kappa_L(T)$. On the basis of the values of $\kappa(T)$, $\alpha(T)$, and $\rho(T)$, the ZT(T) of $SnCCo_3$ (5−330 K) is obtained according to the formula ZT = $\alpha^2T/\rho\kappa$ and illustrated in Figure 3c. The temperature-dependent ZT is similar to that of $\alpha(T)$, reaching its maximum of 0.035(2) around 258 K. This ZT value is the largest among the antiperovskite compounds AXM_3 based on the reported results from the literature.[10,20,25] It is necessary to point out that the ZT value is more than 0.03 in a wide temperature range of 200−330 K, which would favor TE cooling around or below room temperature. As shown in Figure 3d, the ZT value of $SnCCo_3$ [~0.035(2), 258 K] is relatively large compared with those of several typical TE materials such as $ZnC_{1.2}Fe_3$ (~0.012, 170 K), $Co_{0.3}Ti_{0.7}S_2$ (~0.001, 150 K), TiS_2 (~0.0176, 300 K), $LaGdS_3$ (~0.04, 300 K), $BaMn_2Bi_2$ (~0.005, 300 K), $La_{0.04}Sr_{0.96}TiO_3$ (~0.02, 300 K), $CuSbSe_2$ (~0.0024, 310 K), and $La_{0.875}Sr_{0.125}CoO_3$ (~0.035, 230 K).[10,26−31] Therefore, considering its advantages such as a large ZT value with a wide operating temperature range, inexpensive raw materials, and friendly to environment, the Co-based antiperovskite carbide $SnCCo_3$ may be a promising candidate for TE cooling.

In order to further understand the large TE in $SnCCo_3$, other Co-based antiperovskite carbides $ACCo_3$ (A = Al, Ga, Ge) and isostructural carbides $SnCM_3$ (M = Mn, Fe) were synthesized, and the corresponding $\alpha(T)$, $\kappa(T)$, and $\rho(T)$ were measured, which are plotted in parts a−c of Figure 4, respectively. Apparently, $SnCCo_3$ has the largest Seebeck coefficient (see Figure 4a) and electrical resistivity (see Figure 4b) and the smallest thermal conductivity (see Figure 4c) among all of the samples. After calculation according to the formula ZT = $\alpha^2T/\rho\kappa$, the ZT value of $SnCCo_3$ is the largest among all of the studied samples and is plotted in Figure 4d. As displayed in the inset of Figure 4d, the $\rho\kappa(T)$ values of all samples are little different in the whole temperature range. According to the relationship ZT = $\alpha^2T/\rho\kappa$, the largest ZT of $SnCCo_3$ is mainly due to the largest α of $SnCCo_3$ among all of the samples. The largest electrical resistivity of $SnCCo_3$ mainly results from the smallest carrier density n (discussed below) of $SnCCo_3$. As mentioned above, the total thermal conductivity can be expressed as a sum of the lattice (κ_L) and electronic (κ_e) terms, i.e., $\kappa(T) = \kappa_L(T) + \kappa_e(T)$. According to the Keyes rule,[32] materials of high mean atomic weight should have low lattice thermal conductivity for the same series of compounds. Here, for antiperovskite carbides ACM_3 (A = Al, Ga, Ge, Sn; M = Mn, Fe, Co), $SnCCo_3$ has the largest atomic weight among all of the samples; thus, the lattice thermal conductivity of $SnCCo_3$ is the smallest. At the same time, the electronic thermal conductivity is calculated by the WF law ($\kappa_e = L_0T/\rho$, where $L_0 = 2.45 \times 10^{-8}$ W·Ω·K^{-2} is the Lorentz number). The largest electrical resistivity of $SnCCo_3$ leads to the smallest electronic thermal conductivity of $SnCCo_3$. As a result, the smallest electronic and lattice thermal conductivities of $SnCCo_3$ result in the smallest

dx.doi.org/10.1021/ic500026t | Inorg. Chem. 2014, 53, 3709−3715

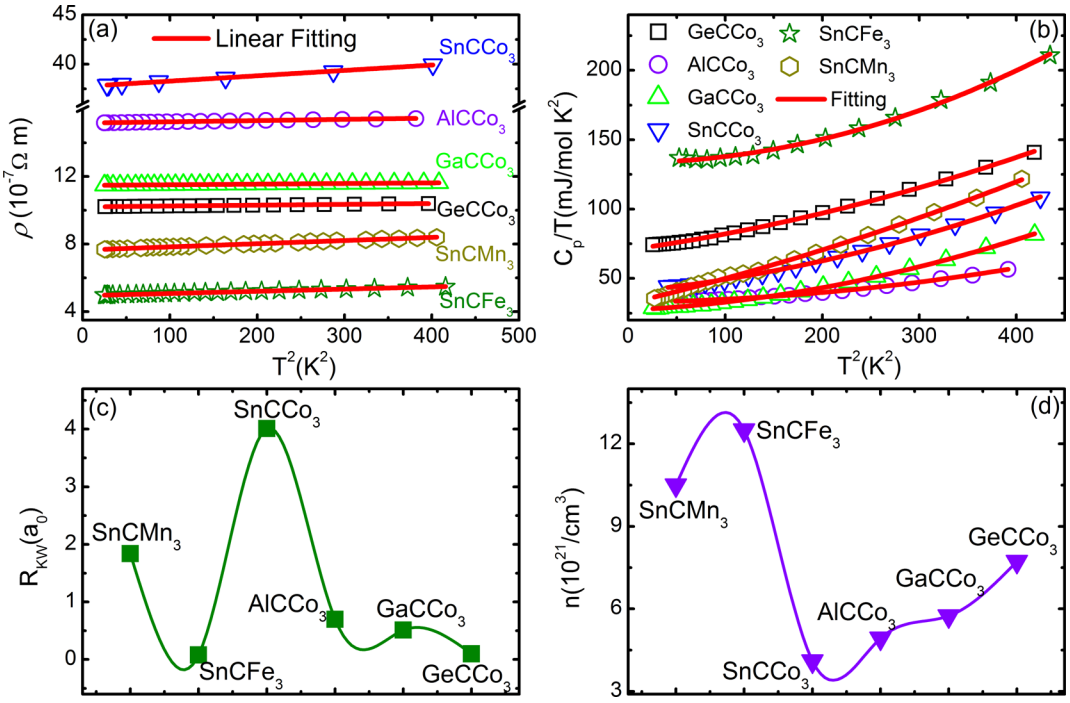

Figure 5. For $SnCM_3$ (M = Mn, Fe, Co) and $ACCo_3$ (A = Sn, Ga, Al, Ge). (a) Lower-T $\rho(T)$ data plotted as $\rho(T)$ versus T^2 between 5 and 20 K. The solid line is the linear fitting result. (b) Plot of $C_P(T)/T$ versus T^2 in the temperature range of 5−20 K. The solid line represents the fitting results according to eq 2. (c) R_{KW} ratio. (d) Carrier density n at room temperature.

Table 1. T^2-Term Coefficient of the Formula $\rho = \rho_0 + AT^2$ (A), Sommerfeld Constant (γ), Kadowaki−Woods Ratio (R_{KW}), and Carrier Concentration at 300 K ($n_{300\ K}$) of $ACCo_3$ (A = Al, Ga, Ge, Sn) and $SnCM_3$ (M = Mn, Fe, Co), Where $a_0 = 10^{-5}$ μΩ·cm/(mJ/mol·K)^2

	$SnCMn_3$	$SnCFe_3$	$SnCCo_3$	$AlCCo_3$	$GaCCo_3$	$GeCCo_3$
$A(10^{-10}$ Ω·m/K$^2)$	1.891(2)	1.292(1)	6.576(5)	0.751(1)	0.376(2)	0.492(4)
γ (mJ/mol·K^2)	32.07(3)	126.97(4)	40.51(2)	32.82(3)	27.15(4)	70.52(2)
R_{KW} (a_0)	1.84(4)	0.08(2)	4.01(2)	0.69(2)	0.51(3)	0.01(1)
$n_{300\ K}$ (10^{21}/cm^3)	10.50(2)	12.50(1)	4.12(3)	4.93(2)	5.74(1)	7.78(2)

thermal conductivity of $SnCCo_3$ among all of the samples. Moreover, such a large Seebeck coefficient α of $SnCCo_3$ is abnormal in antiperovskite compounds. In general, the Seebeck coefficient of an isotropic substance can be modeled as the Mott formula:[20,33,34]

$$\alpha = \frac{\pi^2 k_B{}^2 T}{3q}\left\{\frac{\mathrm{d}[\ln \sigma(E)]}{\mathrm{d}E}\right\}_{E=E_F} = \frac{\pi^2 k_B{}^2 T}{3q}\left\{\frac{1}{n}\frac{\mathrm{d}n(E)}{\mathrm{d}E} + \frac{1}{\mu}\frac{\mathrm{d}\mu(E)}{\mathrm{d}E}\right\}_{E=E_F} \quad (3)$$

where q is the carrier charge, k_B is the Boltzmann constant, E_F is the Fermi energy, and $\sigma(E)$ is the energy-dependent electrical conductivity and equals $n(E)q\mu(E)$ taken at the Fermi energy, $n(E)$ is the carrier density, and $\mu(E)$ is the mobility. For metallic behavior materials or degenerate semiconductor, the Mott equation can be simplified as

$$\alpha = \frac{8\pi^2 k_B{}^2 T}{3qh^2} m^* \left(\frac{\pi}{3n}\right)^{2/3} \quad (4)$$

where h is the Plank constant, n is the carrier density, and m^* is the carrier effective mass, assuming free electron dispersion and energy-independent scattering.[33,34] Here, the magnitude of the Seebeck coefficient is only determined by m^* and n. As reported previously by Merino and McKenzie,[35] a strong electron correlation ($R_{KW} > a_0$) can enhance the effective mass m^* and lead to a large value of the Seebeck coefficient.[35,36] This means that a strong electron correlation is closely related to the effective mass m^*. Parts a and b of Figure 5 present the lower-T $\rho(T)$ data plotted as $\rho(T)$ versus T^2 and the plot of $C_P(T)/T$ versus T^2 below 20 K, respectively, and the solid lines are the fitting results. Obviously, all of the results are fitted well, and the detailed fitting parameters A and γ are listed in Table 1. In terms of the formula $R_{KW} = A/\gamma^2$, R_{KW} values of $SnCM_3$ (M = Mn, Fe, Co) and $ACCo_3$ (A = Al, Ga, Ge, Sn) are obtained and are plotted in Figure 5c. R_{KW} of $SnCCo_3$ is the largest among those of all of the samples. At the same time, as shown in Figure 5d, we also obtained the carrier density n, which is calculated by the formula $n = 1/eR_H$, at room temperature by measuring the Hall coefficient R_H for $SnCM_3$ (M = Mn, Fe, Co) and $ACCo_3$ (A = Al, Ga, Ge, Sn). n of $SnCCo_3$ [~4.12(3) × 10^{21}/cm^3] is the smallest among those of all of the samples. The detailed values of R_{KW} and n are summarized in Table 1. In a word, according to eq 4, the largest Seebeck coefficient of $SnCCo_3$ is mainly due to the combined action of the largest R_{KW} (namely, the largest m^*) and the smallest n among all of the samples of $SnCM_3$ (M = Mn, Fe, Co) and $ACCo_3$ (A = Al, Ga, Ge, Sn).

dx.doi.org/10.1021/ic500026t | Inorg. Chem. 2014, 53, 3709−3715

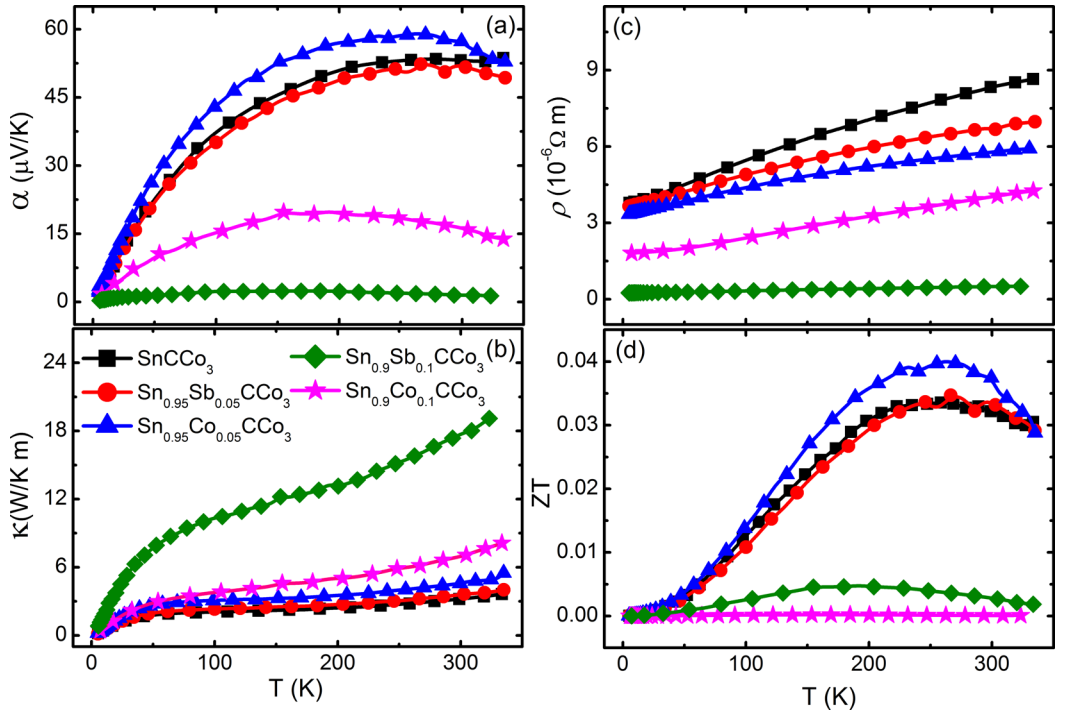

Figure 6. Temperature-dependent $\alpha(T)$, $k(T)$, $\rho(T)$, and ZT(T) curves for $Sn_{1-x}Sb_x(Co_x)CCo_3$ (x = 0, 0.05, and 0.1), respectively: (a) $\alpha(T)$; (b) $k(T)$; (c) $\rho(T)$; (d) ZT(T).

Previous works have confirmed that chemical doping in TE materials is a good way to enhance the ZT value.[33,37,38] Especially for half-Heusler TE materials, for MNiSn (where M can be a transition metal, a noble metal, or a rare-earth element), 0.5−5 atom % Sb replacing Sn is the most effective electron doping, and for MCoSb, 20−30% Sn replacing Sb is the most efficient hole doping.[34] Namely, both electron and hole doping could effectively improve the TE performance in half-Heusler TE materials. Similarly, in order to improve the TE performance of the $SnCCo_3$ system, we synthesized Sb-doping (electron-doping) $Sn_{1-x}Sb_xCCo_3$ (x = 0, 0.05, and 0.1) and Co-doping (hole-doping) $Sn_{1-x}Co_xCCo_3$ (x = 0, 0.05, and 0.1) samples and investigated $\kappa(T)$, $\alpha(T)$, $\rho(T)$, and ZT(T), which are plotted in parts a−d of Figure 6, respectively. For $Sn_{0.95}Co_{0.05}CCo_3$, the Seebeck coefficient increases to 60 μV/K and leads to an increase of the ZT value with a maximum of 0.041(1) around 263 K. It is noted that the ZT value is more than 0.035(2) between 200 and 310 K, which is beneficial for TE cooling around or below room temperature. For $Sn_{0.95}Sb_{0.05}CCo_3$, the Seebeck coefficient and ZT value are basically unchanged compared with those of $SnCCo_3$. However, the ZT values of highly doped (x = 0.1) samples appear to decline, which is mainly attributed to the decrease of the Seebeck coefficient. Besides, both pressure and grain refinement are also effective methods for enhancement of the TE performance.[1,2] We hope our work may stimulate more experiments, especially for the TE performance under high pressure or after grain refinement, and theoretical research on the fascinating material $SnCCo_3$.

4. CONCLUSIONS

In summary, we investigated the magnetic, electrical, and thermal properties of $SnCCo_3$, where a good TE performance [ZT = 0.035(2), 258 K] associated with a strong electron correlation ($R_{KW} = 4a_0$) is observed. The ZT value of $SnCCo_3$ is considerably large compared with other typical nearly room-temperature TE materials. For comparison, we also studied the TE properties of other Co-based antiperovskite carbides $ACCo_3$ (A = Al, Ga, Ge) and isostructural carbides $SnCM_3$ (M = Mn, Fe) and found that the ZT value of $SnCCo_3$ is the largest among those samples, which is mainly attributed to the largest Seebeck coefficient of $SnCCo_3$. According to the simplified Mott formula, the large Seebeck coefficient of $SnCCo_3$ originates from the large carrier effective mass enhanced by a strong electron correlation and the small carrier density. Moreover, in order to enhance the ZT value of the $SnCCo_3$ system, we synthesized the electron-doping (Sb-doping) and hole-doping (Co-doping) samples $Sn_{1-x}Co_x(Sb_x)$-CCo_3. As a result, the ZT value of $Sn_{0.95}Co_{0.05}CCo_3$ increases up to 0.041(1) around 263 K with an increase ratio of 14.3%. However, the ZT values of highly doped samples (x = 0.1) display a decline, which is mainly due to a reduction of the Seebeck coefficient. Finally, considering the advantages of a large ZT value with a wide operating temperature range, inexpensive raw materials, and friendly to the environment, the Co-based antiperovskite carbides $SnCCo_3$ and $Sn_{0.95}Co_{0.05}(Sb_{0.05})CCo_3$ may be promising candidates for TE refrigerant applications.

AUTHOR INFORMATION

Corresponding Authors

*E-mail: tongpeng@issp.ac.cn. Tel: +86-551-6559-2757. Fax: +86-551-6559-1434.

*E-mail: ypsun@issp.ac.cn. Tel: +86-551-6559-2757. Fax: +86-551-6559-1434.

Notes

The authors declare no competing financial interest.

■ ACKNOWLEDGMENTS

This work was supported by the National Key Basic Research under Contract 2011CBA00111, the National Natural Science Foundation of China under Contracts 51301165, 51001094, 51171177, 51371005, 51322105, and 91222109, the Foundation of Hefei Center for Physical Science and Technology under Contract 2012FXCX007, and the Director Fund of the Institute of Solid State Physics, Chinese Academy of Sciences.

■ REFERENCES

(1) Ovsyannikov, S. V.; Shchennikov, V. V. *Chem. Mater.* **2010**, *22*, 635−647.
(2) Szczech, J. R.; Higgins, J. M.; Jin, S. *J. Mater. Chem.* **2011**, *21*, 4037−4055.
(3) Mahan, G. D. *Solid State Phys.* **1998**, *51*, 81−157.
(4) (a) Sun, P. J.; Oeschler, N.; Johnsen, S.; Iversen, B. B.; Steglich, F. *Phys. Rev. B* **2009**, *79*, 153308. (b) Sun, P. J.; Oeschler, N.; Johnsen, S.; Iversen, B. B.; Steglich, F. *Dalton Trans.* **2010**, *39*, 1012−1019.
(5) He, T.; Huang, Q.; Ramirez, A. P.; Wang, Y.; Regan, K. A.; Rogado, N.; Hayward, M. A.; Haas, M. K.; Slusky, J. S.; Inumara, K.; Zandbergen, H. W.; Ong, N. P.; Cava, R. J. *Nature (London)* **2001**, *411*, 54−56.
(6) Wang, B. S.; Tong, P.; Sun, Y. P.; Zhu, X. B.; Yang, Z. R.; Song, W. H.; Dai, J. M. *Appl. Phys. Lett.* **2010**, *97*, 042508.
(7) Kamishima, K.; Goto, T.; Nakagawa, H.; Miura, N.; Ohashi, M.; Mori, N.; Sasaki, T.; Kanomata, T. *Phys. Rev. B* **2000**, *63*, 024426.
(8) Li, Y. B.; Li, W. F.; Feng, W. J.; Zhang, Y. Q.; Zhang, Z. D. *Phys. Rev. B* **2005**, *72*, 024411.
(9) Wang, B. S.; Tong, P.; Sun, Y. P.; Li, L. J.; Tang, W.; Lu, W. J.; Zhu, X. B.; Yang, Z. R.; Song, W. H. *Appl. Phys. Lett.* **2009**, *95*, 222509.
(10) Lin, S.; Wang, B. S.; Lin, J. C.; Huang, Y. N.; Hu, X. B.; Zhao, B. C.; Lu, W. J.; Tong, P.; Song, W. H.; Sun, Y. P. *J. Appl. Phys.* **2011**, *110*, 083914.
(11) Wang, B. S.; Lin, J. C.; Tong, P.; Zhang, L.; Lu, W. J.; Zhu, X. B.; Yang, Z. R.; Song, W. H.; Dai, J. M.; Sun, Y. P. *J. Appl. Phys.* **2010**, *108*, 093925.
(12) Takenaka, K.; Asano, K.; Misawa, M.; Takagi, H. *Appl. Phys. Lett.* **2008**, *92*, 011927.
(13) Huang, R. J.; Li, L. F.; Cai, F. S.; Xu, X. D.; Qian, L. H. *Appl. Phys. Lett.* **2008**, *93*, 081902.
(14) Asano, K.; Koyama, K.; Takenaka, K. *Appl. Phys. Lett.* **2008**, *92*, 161909.
(15) Chi, E. O.; Kim, W. S.; Hur, N. H. *Solid State Commun.* **2001**, *120*, 307−310.
(16) Takenaka, K.; Ozawa, A.; Shibayama, T.; Kaneko, N.; Oe, T.; Urano, C. *Appl. Phys. Lett.* **2011**, *98*, 022103.
(17) Lin, S.; Wang, B. S.; Lin, J. C.; Huang, Y. N.; Lu, W. J.; Zhao, B. C.; Tong, P.; Song, W. H.; Sun, Y. P. *Appl. Phys. Lett.* **2012**, *101*, 011908.
(18) Kimura, Y.; Sakai, K.; Mishima, Y. *J. Phase Equilib. Diffus.* **2006**, *27*, 14−21.
(19) Kimura, Y.; Sakai, K.; Wei, F. G.; Mishima, Y. *Intermetallics* **2006**, *14*, 1262−1269.
(20) Maruoka, T.; Suzuki, R. O. *Mater. Trans.* **2006**, *47*, 1422−1427.
(21) L'Héritier, Ph.; Fruchart, D.; Madar, R.; Fruchart, R. In *1.5.6.2 Crystallographic properties of M{c}XM{f}{3} compounds*. Wijn, H. P. J., Ed.; Springer Materials—The Landolt−Börnstein Database (http://www.springermaterials.com). DOI: 10.1007/10353201_69.
(22) Tong, P.; Sun, Y. P.; Zhu, X. B.; Song, W. H. *Phys. Rev. B* **2006**, *73*, 245106.
(23) Kadowaki, K.; Woods, S. B. *Solid State Commun.* **1986**, *58*, 507−509.
(24) Siebold, Th.; Ziemann, P. *Phys. Rev. B* **1995**, *51*, 6328−6335.
(25) Lin, S.; Tong, P.; Wang, B. S.; Huang, Y. N.; Shao, D. F.; Lu, W. J.; Sun, Y. P. *J. Solid State Chem.* **2014**, *209*, 127−134.
(26) Zhang, J.; Qin, X. Y.; Xin, H. X.; Li, D.; Song, C. J. *J. Electron. Mater.* **2011**, *40*, 980−986.
(27) Ohat, M.; Hirai, S.; Kuzuya, T. *J. Electron. Mater.* **2011**, *40*, 537−542.
(28) Shang, P. P.; Zhang, B. P.; Liu, Y.; Li, J. F.; Zhu, H. M. *J. Electron. Mater.* **2011**, *40*, 926−931.
(29) Li, D.; Qin, X. Y. *J. Appl. Phys.* **2006**, *100*, 023713.
(30) Berggold, K.; Kriener, M.; Zobel, C.; Reichl, A.; Reuther, M.; Muller, R.; Freimuth, A.; Lorenz, T. *Phys. Rev. B* **2005**, *72*, 155116.
(31) Wang, K. F.; Petrovic, C. *Appl. Phys. Lett.* **2013**, *103*, 192104.
(32) Nolas, G. S.; Sharp, J.; Goldsmid, H. J. *Thermoelectrics: Basic Principles and New Materials Developments*; Springer: New York, 2001.
(33) Heremans, J. P.; Jovovic, V.; Toberer, E. S.; Saramat, A.; Kurosaki, K.; Charoenphakdee, A.; Yamanaka, S.; Snyder, G. J. *Science* **2008**, *321*, 554−557.
(34) Chen, S.; Ren, Z. F. *Mater. Today* **2013**, *16*, 387−395.
(35) Merino, J.; McKenzie, R. H. *Phys. Rev. B* **2000**, *61*, 7996−8008.
(36) Wang, Y.; Sui, Y.; Ren, P.; Wang, L.; Wang, X. J.; Su, W. H.; Fan, H. J. *Chem. Mater.* **2010**, *22*, 1155−1163.
(37) Kudo, K.; Nakano, S.; Mizukami, T.; Takabatake, T.; Nohara, M. *Appl. Phys. Lett.* **2013**, *103*, 092107.
(38) Usui, H.; Suzuki, K.; Kuroki, K.; Nakano, S.; Kudo, K.; Nohara, M. *Phys. Rev. B* **2013**, *88*, 075140.